

The P2X7 receptor–pannexin-1 complex decreases muscarinic acetylcholine receptor–mediated seizure susceptibility in mice

Ji-Eun Kim and Tae-Cheon Kang

Department of Anatomy and Neurobiology, Institute of Epilepsy Research, College of Medicine, Hallym University, Chunchon, South Korea.

Pannexin-1 (Panx1) plays a role in the release of ATP and glutamate in neurons and astrocytes. Panx1 can be opened at the resting membrane potential by extracellular ATP via the P2X7 receptor (P2X7R). Panx1 opening has been shown to induce neuronal death and aberrant firing, but its role in neuronal activity has not been established. Here, we report the role of the P2X7R–Panx1 complex in regulating muscarinic acetylcholine 1 (M1) receptor function. P2X7R knockout ($P2X7^{-/-}$) mice showed greater susceptibility to seizures induced by pilocarpine (PILO), an M1 receptor agonist, than their WT littermates, despite having similar levels of hippocampal M1 receptor expression. This hypersensitivity to PILO in the $P2X7^{-/-}$ mice did not involve the GABA or glutamate system. Both administration of P2X7R antagonists and gene silencing of P2X7R or Panx1 in WT mice increased PILO-induced seizure susceptibility in a process mediated by PKC via intracellular Ca^{2+} release. Therefore, we suggest that the P2X7R–Panx1 complex may play an important role as a negative modulator of M1 receptor–mediated seizure activity in vivo.

Introduction

The P2X receptors are a family of cation-permeable ligand-gated ion channels that open in response to binding of extracellular ATP. Among them, the P2X7 receptors (P2X7Rs) function through the formation of membrane pores that are permeable to ions and large molecules (Ca^{2+} and ATP). P2X7R is a unique channel in that its activation not only opens a typical ion channel, but also gradually opens pannexin-1 (Panx1) for passage of molecules up to 900 Da (1–4). Panx1 is a vertebrate homolog of the invertebrate innexin gap junction proteins (5). However, Panx1 does not form functional gap junctions, but acts as a channel that carries ions and signaling molecules between the cytoplasm and extracellular space (6, 7). Panx1 plays a role in releasing ATP and glutamate in neurons and astrocytes. Panx1 channels can be opened at the resting membrane potential by extracellular ATP via P2X7R. Prolonged or repeated activation of Panx1 by ATP binding to P2X7R results in cell death (3). Thus, Panx1 is the molecular substrate for the channel recruited into the P2X7R death complex.

Recently, it has been reported that the opening of Panx1 induces neuronal death and aberrant bursting in vitro (8, 9). Thus, Panx1 is considered an important target for treatment of neurological disorders, such as stroke and epilepsy. Interestingly, prolonged and/or repeated Panx1 activation via P2X7R induces cell death, but only Panx1 opening does not (10). However, the role of the P2X7R–Panx1 complex in neuronal activity is unknown. Here, we demonstrate that deletion and/or blockade of P2X7R and knockdown of Panx1 increased seizure susceptibility in response to activation of the muscarinic acetylcholine 1 (M1) receptor induced by pilocarpine (PILO), an M1 receptor agonist. We suggest that the P2X7R–Panx1 complex may prove to be an essential negative modulator of M1 receptor–mediated seizure activity in vivo.

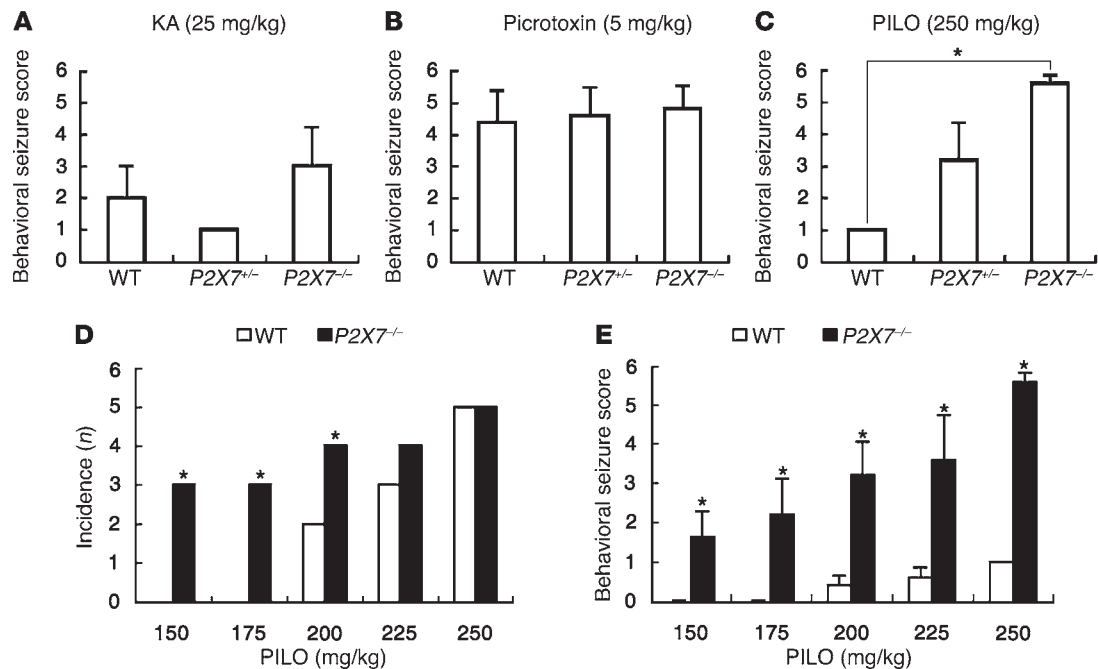
Results

P2X7^{-/-} mice show increased PILO-induced seizure susceptibility. Within 15–30 minutes of treatment with kainic acid (KA, 25 mg/kg i.p.) or picrotoxin (5 mg/kg i.p.), WT, $P2X7^{+/+}$, and $P2X7^{-/-}$ mice became catatonic and began staring, followed by myoclonic twitching and often frequent rearing and falling. The seizures were sometimes fatal. There was no difference in the behavioral seizure score induced by KA or picrotoxin among the 3 groups (Figure 1, A and B). After PILO administration (250 mg/kg i.p.), all WT mice (5 of 5) and most $P2X7^{+/+}$ mice (3 of 5) were immobilized for less than 3 hours. The $P2X7^{-/-}$ mice showed severe seizure activity in response to PILO compared with WT mice. At 15–20 minutes after PILO administration, all of the $P2X7^{-/-}$ mice showed seizure activity (seizure score, ≥ 2). The $P2X7^{-/-}$ mice died during seizure within 1 hour (3 of 5) or experienced continuous seizure activity for more than 3 hours (2 of 5; $P < 0.05$; Figure 1C). To detail the seizure susceptibility of $P2X7^{-/-}$ mice in response to PILO, we investigated seizure incidence and behavioral seizure score in response to various doses of PILO (150, 175, 200, 225, or 250 mg/kg i.p.). At each dose, the incidence of seizure or behavioral seizure score in $P2X7^{-/-}$ mice was higher than that in WT mice. In addition, 60% of $P2X7^{-/-}$ mice showed seizure activity in response to nonconvulsive doses of PILO (150 and 175 mg/kg), compared with none of the WT mice ($P < 0.05$, Figure 1, D and E).

To quantify the change in seizure threshold in $P2X7^{-/-}$ mice, we recorded electroencephalograms (EEGs) after treatment with 250 mg/kg PILO i.p. There was no difference in basal EEG between WT and $P2X7^{-/-}$ animals. WT and $P2X7^{-/-}$ animals had root mean square values of 0.63 ± 0.24 and 0.46 ± 0.23 mV, respectively (Figure 2, A and B). After PILO injection, the WT mice showed γ -oscillation (a synchronous neuronal activity in a frequency band between 30 and 80 Hz; ref. 11) without epileptiform discharge (Figure 2A). However, $P2X7^{-/-}$ mice showed epileptiform discharges at 6.31 ± 3.28 minutes after PILO injection (Figure 2B). At 11 minutes after PILO injection, the normalized power value also increased to 1.96-fold of the control ($P < 0.05$; Figure 2, B and C).

Conflict of interest: The authors have declared that no conflict of interest exists.

Citation for this article: *J Clin Invest.* 2011;121(5):2037–2047. doi:10.1172/JCI44818.

**Figure 1**

Behavioral seizure activity of convulsants in WT and *P2X7*^{-/-} mice. (A) KA-, (B) picrotoxin-, and (C) PILO-induced behavioral seizure scores in WT, *P2X7*^{+/-}, and *P2X7*^{-/-} mice. (D) Incidence of behavioral seizure and (E) behavioral seizure score in response to various doses of PILO in WT and *P2X7*^{-/-} mice. *n* = 5 per group. **P* < 0.05 vs. WT. (A–C and E) Data are mean ± SEM. (D) The number of animals showing behavioral seizure.

Because the M1 receptor mediates PILO-induced seizure activity (12), we investigated whether a difference in M1 receptor expression affects the PILO-induced seizure threshold. There was no difference in M1 receptor expression level in the hippocampus between WT and *P2X7*^{-/-} animals (Figure 2, D–G). Taken together, our findings indicate that *P2X7*^{-/-} mice may be more sensitive to PILO than are WT mice, without alteration in M1 receptor expression.

Increased PILO-induced seizure susceptibility in P2X7^{-/-} mice is unrelated to GABAergic or glutamatergic transmission. To determine whether alteration in GABAergic or glutamatergic transmission increases PILO-induced seizure susceptibility in *P2X7*^{-/-} mice, we compared the paired-pulse responses of the dentate gyrus in WT and *P2X7*^{-/-} animals. In both WT and *P2X7*^{-/-} animals, a single population spike was detected in response to the first stimulus. There was no difference in input-output (IO) curves between WT and *P2X7*^{-/-} animals (Figure 3, A–F). Both WT and *P2X7*^{-/-} mice showed strong paired-pulse depressions at 20- and 30-ms interstimulus intervals. They also showed paired-pulse facilitations at 70-, 150-, and 250-ms interstimulus intervals. There were no differences in the normalized population spike amplitude ratios (second population spike amplitude/first population spike amplitude) at any interstimulus interval between WT and *P2X7*^{-/-} animals (Figure 3G). Similarly, there was no difference in levels of vesicular glutamate transporter 1 (VGLUT1) or vesicular GABA transporter (VGAT) in the hippocampus between the groups (Figure 3, H–K). These results suggest that the increased PILO-induced seizure susceptibility in *P2X7*^{-/-} mice may not involve GABAergic or glutamatergic transmission.

P2X7R antagonists increase PILO-induced seizure susceptibility in WT mice. To directly determine the effect of P2X7R on PILO-induced

seizure susceptibility, 2'(3')-O-(4-benzoyl)benzoyl adenosine 5'-triphosphate (BzATP; a P2X7R agonist), oxidized ATP (OxATP; a nonselective P2X7R antagonist), 3-[5-(2,3-dichlorophenyl)-1H-tetrazol-1-ylmethyl]pyridine hydrochloride (A438079; a selective P2X7R antagonist), or N-(1-[(cyanoimino)(5-quinolinylamino)methyl]amino)-2,2-dimethylpropyl)-2-(3,4-dimethoxyphenyl)acetamide (A740003; a selective P2X7R antagonist) was infused into WT and *P2X7*^{-/-} animals for 1 week prior to the PILO injections. BzATP infusion did not affect PILO-induced behavioral seizure scores in WT mice compared with saline infusion (Figure 4A). However, OxATP, A438079, and A740003 infusion increased PILO-induced seizure susceptibility in WT mice to levels observed in saline-infused *P2X7*^{-/-} mice (*P* < 0.05 vs. saline- or vehicle-infused WT, Figure 4A; *P* = 0.43, 0.39, and 0.50, respectively, vs. saline-infused *P2X7*^{-/-} mice, data not shown). Neither BzATP nor the P2X7R antagonists affected PILO-induced behavioral seizure scores in the *P2X7*^{-/-} animals (data not shown).

Similarly, OxATP, A438079, and A740003 infusion induced epileptiform discharge in WT mice at 13.30 ± 2.92, 12.46 ± 3.98, and 10.46 ± 4.12 minutes after PILO injection, respectively, without alterations in basal EEGs (Figure 4B). OxATP, A438079, and A740003 infusion increased the normalized power value to 2.69-, 2.58-, and 2.65-fold of the control, respectively, at 11 minutes after PILO injection (*P* < 0.05 vs. saline- or vehicle-infused WT, Figure 4C; *P* = 0.38, 0.46, and 0.33, respectively, vs. saline-infused *P2X7*^{-/-}, data not shown). Neither the P2X7R agonist nor the P2X7R antagonists affected the time point of PILO-induced seizure onset in *P2X7*^{-/-} animals (data not shown). These findings indicate that PILO-induced seizure hypersusceptibility in *P2X7*^{-/-} mice may be a direct response to *P2X7* gene deletion.

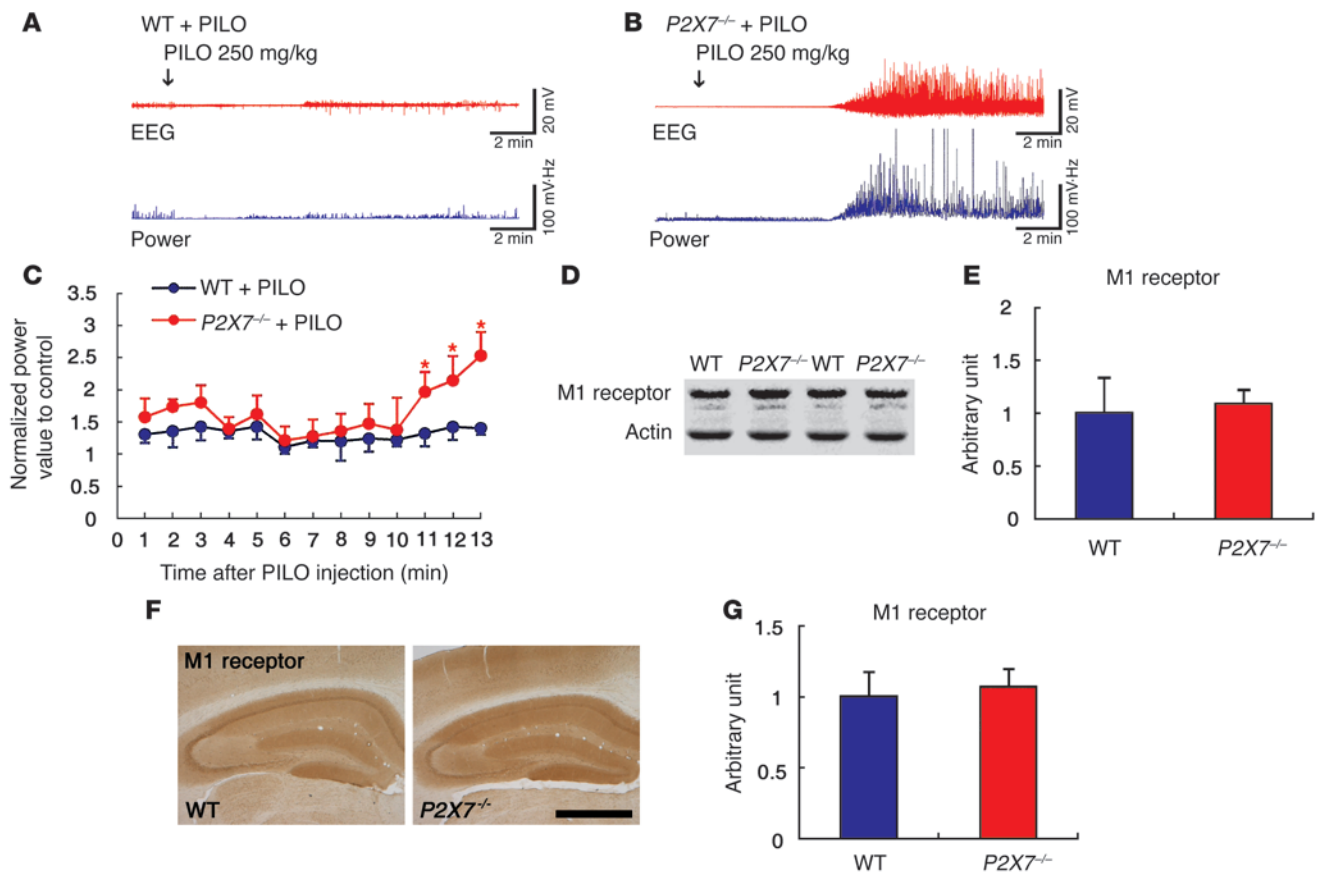


Figure 2

PILO-induced seizure susceptibility in WT and *P2X7^{-/-}* mice. (A and B) EEG and power values for WT (A) and *P2X7^{-/-}* (B) mice after PILO injection. (C) Power values after PILO injection, normalized to control ($n = 7$). * $P < 0.05$ vs. WT. (D) Protein expression for the M1 receptor in WT and *P2X7^{-/-}* mice. (E) Optical density of the M1 receptor, based on Western blotting ($n = 5$). (F) M1 receptor immunoreactivity in the hippocampus of WT and *P2X7^{-/-}* mice. Scale bar: 400 μm . (G) Optical density of the M1 receptor, based on immunohistochemistry ($n = 5$). Data are mean \pm SEM.

Blockade of Panx1 function increases PILO-induced seizure susceptibility in WT mice. Because P2X7R interacts with Panx1 (3, 4), it is possible that Panx1 function increases seizure susceptibility in *P2X7^{-/-}* mice. Indeed, carbenoxolone (CBX; a nonselective Panx1 blocker) and probenecid (PBN; a selective Panx1 blocker) show anticonvulsant effects in various seizure models (13, 14). To evaluate the effect of Panx1 function on the PILO-induced seizure threshold, WT and *P2X7^{-/-}* animals were administered Panx1 blockers prior to PILO injection. Unexpectedly, pretreatment with 30 mg/kg CBX or PBN increased the PILO-induced behavioral seizure score in WT animals ($P < 0.05$ vs. saline, Figure 5A). CBX and PBN pretreatment also induced an increase in the normalized power value to 2.24- and 2.44-fold of control, respectively, at 11 minutes after PILO injection ($P < 0.05$, Figure 5, B, C, and F). In *P2X7^{-/-}* mice, neither CBX nor PBN pretreatment affected behavioral seizure score, basal EEG, time of seizure onset, or normalized power value induced by PILO (Figure 5, A, D, E, and G).

To evaluate whether altered Panx1 expression level affects the PILO-induced seizure threshold in *P2X7^{-/-}* mice, we performed immunohistochemistry and Western blot tests for Panx1. Panx1 immunoreactivity was present in the majority of the principal cells

(pyramidal cells and dentate granule cells) and interneurons and was also detected in astroglia (Figure 6A). There was no difference in Panx1 expression level or its localization in the hippocampus between WT and *P2X7^{-/-}* animals (Figure 6, A–D).

To confirm the effect of Panx1 on the PILO-induced seizure threshold, we conducted Panx1 knockdown experiments in WT and *P2X7^{-/-}* mice. At 2 weeks after *Panx1* siRNA infusion, Panx1 expression in the hippocampi of WT and *P2X7^{-/-}* mice was reduced, but there was no difference between groups in the degree of Panx1 knockdown (Figure 6D). In WT mice, however, *Panx1* siRNA infusion increased the normalized power value to 2.92-fold of control at 11 minutes after PILO injection ($P < 0.05$, Figure 6, E and F). Control siRNA infusion did not affect the normalized power value after PILO injection (Figure 6F). In *P2X7^{-/-}* mice, Panx1 knockdown did not affect the PILO-induced seizure susceptibility (data not shown). These results indicate that reduced Panx1 function may increase susceptibility to PILO-induced seizures in *P2X7^{-/-}* mice.

Blockade of intracellular Ca²⁺ release reduces PILO-induced seizure susceptibility. Since PILO induces seizure activity via increased intracellular Ca²⁺ release (ICR) (11, 12), we investigated expression levels of the inositol-1,4,5 trisphosphate (IP3) receptor, the

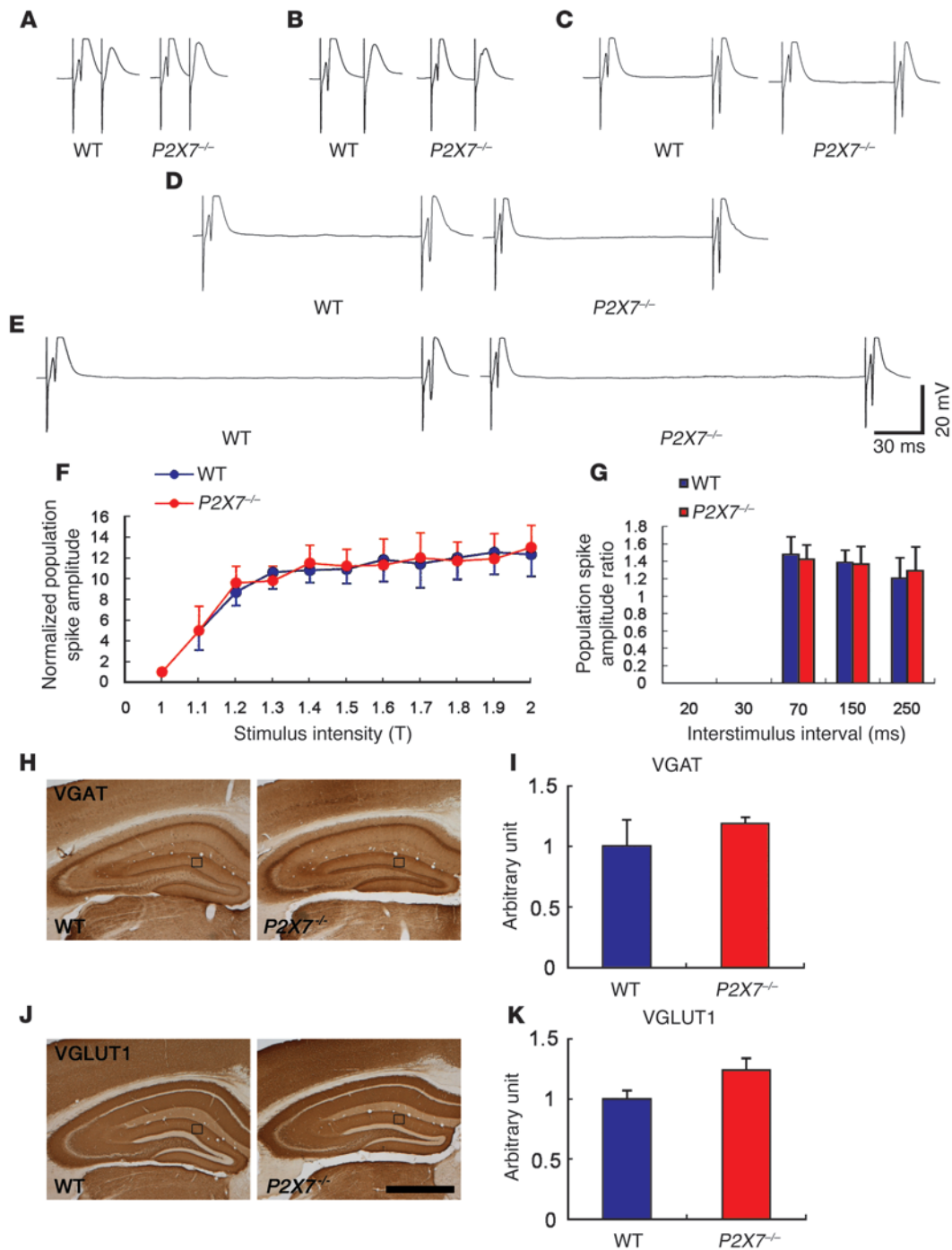
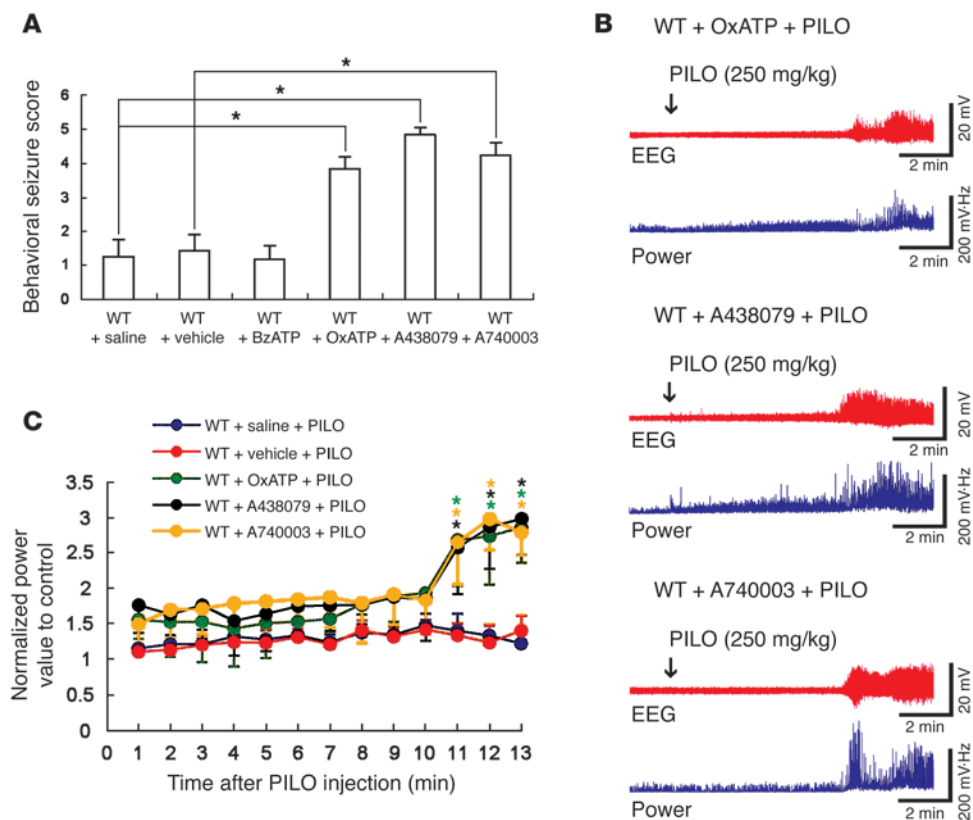


Figure 3

GABAergic and glutamatergic transmission in the dentate gyrus of WT and *P2X7*^{-/-} mice. (A–E) Paired-pulse responses in the dentate gyrus of WT and *P2X7*^{-/-} mice at (A) 20-, (B) 30-, (C) 70-, (D) 150-, and (E) 250-ms interstimulus intervals. (F) IO curves for the dentate gyrus of WT and *P2X7*^{-/-} mice (*n* = 5). (G) Normalized population spike amplitude ratios in the dentate gyrus (*n* = 5). (H–J) Immunoreactivity of (H) VGAT and (J) VGLUT1 in WT and *P2X7*^{-/-} mice. Boxed regions denote the measured areas for immunodensity. Scale bar: 400 μm. Optical density of (I) VGAT and (K) VGLUT1 immunoreactivity, based on immunohistochemistry (*n* = 5). Data are mean ± SEM.

ryanodine receptor, and sarcoplasmic or endoplasmic reticulum calcium ATPase 2 (SERCA2) in the hippocampi of WT and *P2X7*^{-/-} mice (Figure 7, A–J). There was no difference in IP3 receptor, ryanodine receptor, and SERCA2 expression between WT and

P2X7^{-/-} mice. However, pretreatment with 2-aminoethyl diphenylborinate (2-APB; an IP3 receptor antagonist) effectively reduced PILO-induced seizure susceptibility in *P2X7*^{-/-} mice (*P* < 0.05, Figure 7, K and L). Moreover, pretreatment with dantrolene

**Figure 4**

Effect of P2X7R antagonist infusion on PILO-induced seizure susceptibility in WT mice. **(A)** Effect of P2X7R antagonists on behavioral seizure score ($n = 7$). $*P < 0.05$. **(B)** EEGs and power values for P2X7R antagonist-infused WT mice after PILO injection. **(C)** Power values after PILO injection, normalized to control ($n = 7$). $*P < 0.05$, OxATP and A438079 vs. saline and A740003 vs. vehicle. Data are mean \pm SEM.

(DAN; a ryanodine receptor antagonist) also reduced PILO-induced seizure susceptibility in $P2X7^{-/-}$ mice (data not shown). These findings suggest that IP3 receptor-mediated ICR may be related to PILO-induced seizure susceptibility in $P2X7^{-/-}$ mice.

PKC regulates the function of the P2X7R-Panx1 complex. Although Src tyrosine kinase mediates activation of Panx1 through P2X7R (15), the signal transduction molecule in this pathway is still unknown. Since PILO injection induces PKC expression via ICR in the hippocampus 2 hours after PILO injection (16, 17), PKC is involved in one of the early PILO-related signal pathways in the brain. Therefore, we investigated the role of PKC in PILO-induced seizure susceptibility in $P2X7^{-/-}$ mice. Pretreatment with bisindolylmaleimide (BIM; a PKC inhibitor) 3 days before PILO injection decreased PILO-induced seizure susceptibility in $P2X7^{-/-}$ mice ($P < 0.05$, Figure 8, A and B). Additional PBN treatment 13 minutes after PILO injection induced seizure activity, returning the normalized power value to the level of saline-infused $P2X7^{-/-}$ mice (Figure 8, C and D). In WT mice, BIM infusion did not affect PILO-induced seizure susceptibility (data not shown). These findings indicate that PKC activation via IP3 receptor-mediated ICR may reduce Panx1 function, resulting in PILO-induced seizure hypersensitivity in $P2X7^{-/-}$ mice.

Discussion

Activation of the P2X7R-Panx1 complex is involved in processing of proinflammatory cytokines (4, 18) and in release of ATP

from several cell types, including astrocytes (19, 20), erythrocytes (21), and taste bud cells (22). Long-lasting gating of Panx1 also causes aberrant ionic currents and dysregulated neuronal firing patterns by increasing Ca^{2+} entry (9). In addition, the Panx1-mediated ionic current is disexcited by P2X7R antagonists (10). Therefore, we initially hypothesized that blockade or deletion of P2X7R could attenuate seizure activity or decrease seizure susceptibility. In the present study, however, we found that P2X7R deletion and blockade increased PILO-induced seizure susceptibility via nonglutamatergic and nonGABAergic transmission. Furthermore, inhibition of Panx1 increased PILO-induced seizure susceptibility in WT mice, but not in $P2X7^{-/-}$ mice. M1 receptor activation results in initial accumulation of intracellular IP3 concentrations, which in turn increases the intracellular Ca^{2+} concentration (11, 12). Like connexins, Panx1 and P2X7R contribute to Ca^{2+} wave propagation by transfer of IP3 and ATP-induced ATP release independent of extracellular Ca^{2+} (23–33). Indeed, CBX accelerates NMDA-induced membrane depolarization with a concomitant rise in intracellular Ca^{2+} in vitro (34). Although the high dosage of CBX was needed because of its partial exclusion by the blood-brain barrier (35, 36), the present data also showed that CBX increased PILO-induced seizure susceptibility in WT mice. Thus, it is likely that Panx1 inhibition results in M1 receptor-mediated neuronal hyperexcitability via accumulation of IP3 and blockade of Ca^{2+} wave and ATP release. Furthermore, P2X7R activation results in heterolo-

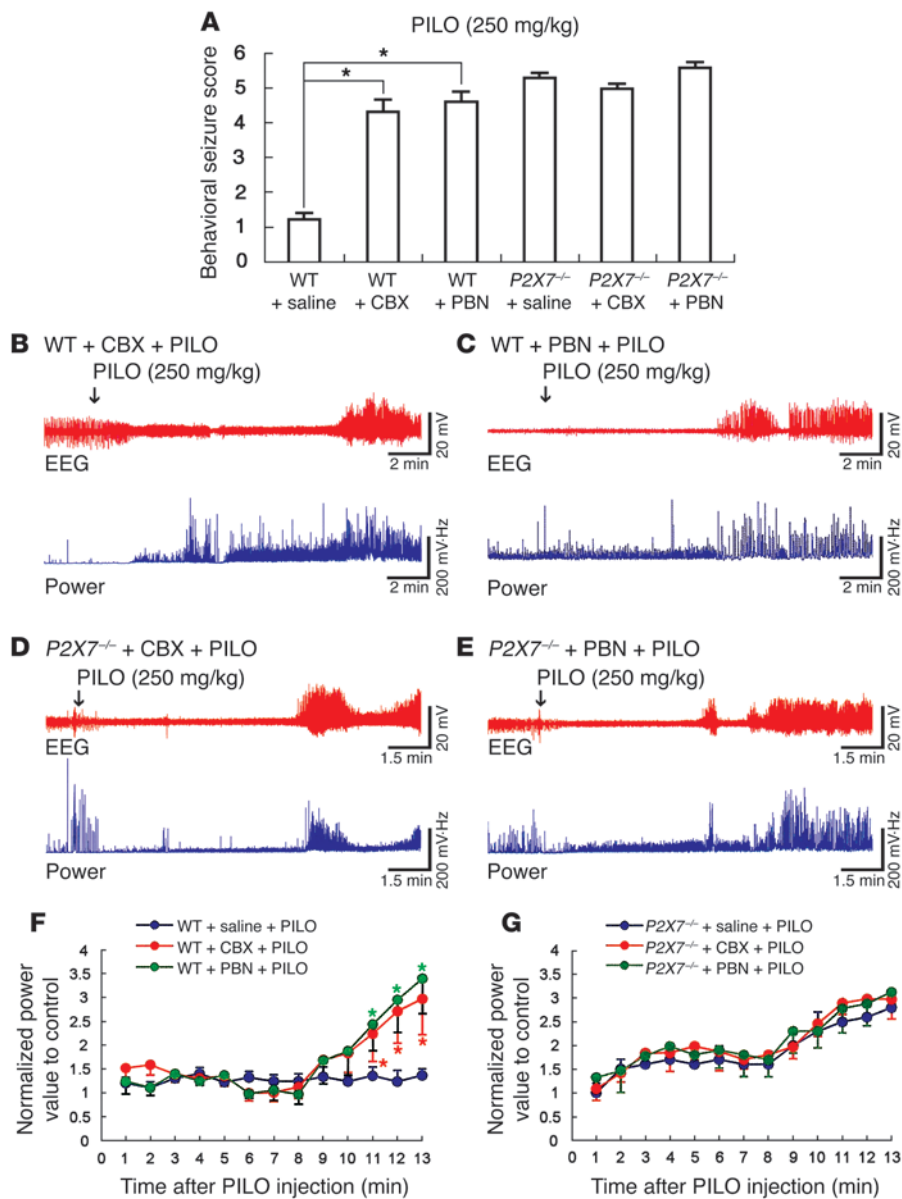
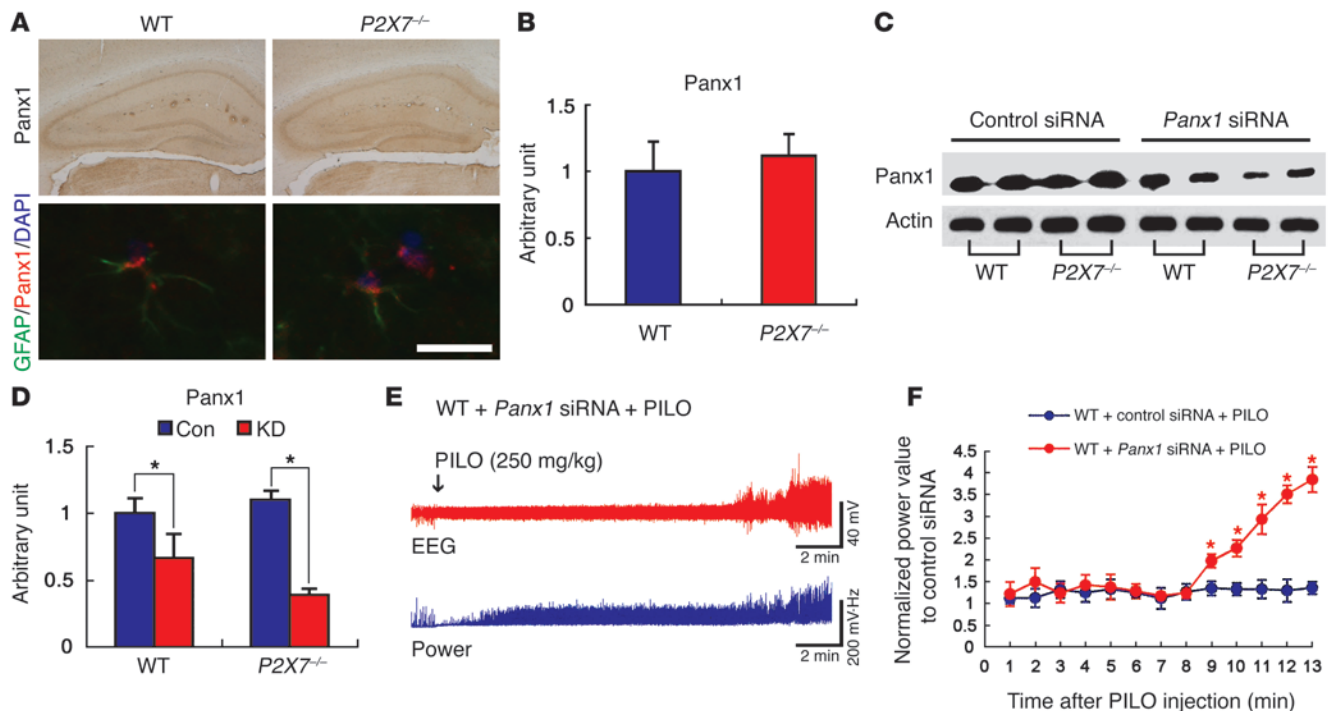


Figure 5 Effect of Panx1 inhibition on PILO-induced seizure susceptibility in WT mice. **(A)** Effect of Panx1 blockers on behavioral seizure score in WT and *P2X7*^{-/-} mice (*n* = 5). **P* < 0.05. **(B and C)** EEGs and power values for CBX- **(B)** and PBN-pretreated **(C)** WT mice after PILO injection. **(D and E)** EEGs and power values for CBX- **(D)** and PBN-pretreated **(E)** *P2X7*^{-/-} mice after PILO injection. **(F and G)** Power values after PILO injection in WT **(F)** and *P2X7*^{-/-} **(G)** mice, normalized to control (*n* = 5). **P* < 0.05 vs. saline. Data are mean ± SEM.

gous desensitization and inhibition of the M1 receptor in the salivary glands (32, 33). Taken together, our findings indicate that blockade or ablation of P2X7R and/or Panx1 may increase the duration and magnitude of M1 receptor-mediated ICR, increasing seizure susceptibility.

Since depolarization gating of Panx1-mediated ionic currents is disexcited by P2X7R antagonists (10), P2X7R-mediated signals regulate Panx1 opening. However, the exact mechanism is still unknown. In the case of gap junction, phosphorylation of connexin by various kinases regulates its permeability (37–39). M1 receptor or P2X7R activation increases intracellular Ca²⁺ signaling, which regulates PKC activity (40, 41). Thus, the PKC

pathway is one of the possible signal transduction pathways involved in modulation of Panx1-P2X7R interactions. In the present study, inhibition of ICR by 2-APB or DAN pretreatment reduced PILO-induced seizure susceptibility in *P2X7*^{-/-} mice. Furthermore, inhibition of PKC by BIM infusion decreased PILO-induced seizure susceptibility in *P2X7*^{-/-} mice to that of WT animals. This inhibitory effect of BIM was offset by additional treatment with PBN. With respect to dephosphorylation-induced opening of gap junctions (37–39), our results indicate that PKC activation via IP3 receptor-mediated ICR may inhibit opening of Panx1, reducing PILO-induced seizure threshold in *P2X7*^{-/-} mice.

**Figure 6**

Effect of silencing *Panx1* mRNA on PILO-induced seizure susceptibility in WT mice. (A) Panx1 immunoreactivity and double immunofluorescent staining for GFAP, Panx-1, and DAPI (counterstain) in WT and *P2X7*^{-/-} mice. Scale bar: 400 μ m (Panx1 immunoreactivity); 12 μ m (double immunofluorescence). (B) Optical density of Panx1 immunoreactivity, based on immunohistochemistry ($n = 5$). (C) Effect of silencing *Panx1* mRNA in WT and *P2X7*^{-/-} mice. (D) Optical density of Panx1 immunoreactivity, based on Western blotting ($n = 5$). Con, control siRNA; KD, *Panx1* siRNA. * $P < 0.05$. (E) Effect of silencing *Panx1* mRNA on EEGs and power values in WT mice after PILO injection. (F) Power values after PILO injection, normalized to control ($n = 5$). * $P < 0.05$ vs. control siRNA. Data are mean \pm SEM.

The results of the present study suggest that in WT animals (Figure 9A), M1 receptor activation triggers IP3 production and increases ICR. Elevated intracellular Ca^{2+} contributes to opening Panx1. Opening Panx1 allows IP3 clearance, Ca^{2+} wave propagation, and ATP release. Releasing ATP through Panx1 activates P2X7R, which desensitizes the M1 receptor and sustains Panx1 opening for clearance of IP3. In turn, PKC activation induced by increased intracellular Ca^{2+} leads to closure of P2X7R and Panx1. In *P2X7*^{-/-} mice (Figure 9B), M1 receptor activation triggers ICR via IP3 production. Elevated intracellular Ca^{2+} contributes to opening Panx1. However, in the absence of P2X7R, Panx1 opening and M1 receptor desensitization cannot be sustained. Simultaneously, PKC activation rapidly closes the Panx1 channel. This condition results in accumulation of intracellular IP3 and prolonged M1 receptor activation, and in turn induces neuronal hyperexcitability via accelerated IP3 receptor-mediated ICR, evoking seizure activity. Thus, our findings suggest that the P2X7R-Panx1 complex plays an important role as a negative modulator of M1 receptor activity via IP3 clearance and ATP release.

Methods

Experimental animals and chemicals. The animals used in the present study were 60- to 90-day-old male WT C57BL/6J mice and male *P2X7*^{-/-} mice (The Jackson Laboratory). Animals were provided a commercial diet and water ad libitum under controlled temperature, humidity, and lighting conditions (22 $^{\circ}$ C \pm 2 $^{\circ}$ C, 55% \pm 5% humidity, and 12-hour light/12-hour dark cycle). Animal protocols were approved by the Institutional Animal

Care and Use Committee of Hallym University. The number of animals used and their suffering was minimized in all cases. All reagents were obtained from Sigma-Aldrich unless otherwise indicated.

Surgery. Mice were anesthetized (50 mg/kg Zoletil or 10 mg/kg Rompun i.p.) and placed in a stereotaxic frame. A hole was drilled through the skull to introduce a cannula. Each animal was implanted with a stainless steel cannula (Brain Infusion Kit 3; Alzet) inserted into the lateral cerebral ventricle 1.0 mm lateral to the bregma. The intracranial part of the cannula was located 2.5 mm below the skull surface, and the extracranial part was connected to an Alzet osmotic minipump (model 1007D, 1003D, or 1002; see below) with a polyurethane catheter. Minipumps were implanted subcutaneously in the midscapular region of the back. Before implantation, the minipumps were filled with one of the investigative compounds and prepared according to the manufacturer's instructions, so that chronic infusions began just after implantation.

Drug and siRNA oligonucleotide infusion. For regulation of P2X7R function, BzATP (5 mM in saline), OxATP (5 mM in saline), A-438079 (10 μ M in saline; Tocris Bioscience), A740003 (10 μ M in 0.001% DMSO/saline, v/v; Santa Cruz Biotechnology Inc.), saline, or vehicle (0.1% DMSO/saline, v/v) was delivered over 1 week using model 1007D osmotic minipumps. For regulation of PKC, BIM (100 μ M in saline) or saline was delivered over 3 days using model 1003D osmotic minipumps. For knockdown of Panx1, siRNA corresponding to the mouse *Panx1* sequence (Ambion Inc.) was infused over 2 weeks using model 1002 osmotic minipumps (0.35 mg/d siRNA in saline). The 3 sequences of siRNA used were as follows: (a) sense, 5'-GGAACUUGACAAGUCUACTT-3'; antisense, 5'-GUAGACUUUGU-CAAGUUCCTC-3'; (b) sense, 5'-GGUGCUGGAGAACAUAATT-3'; anti-

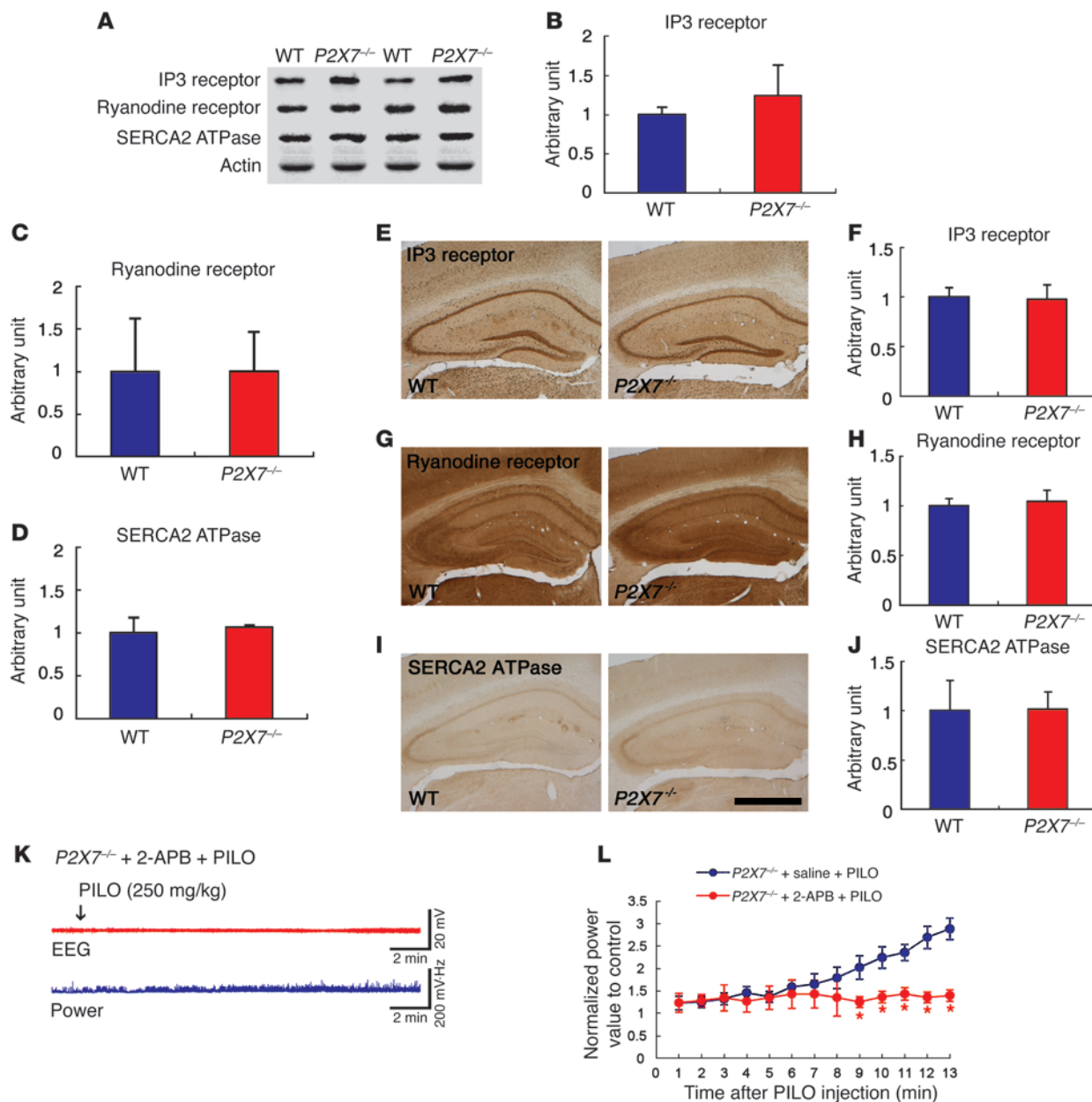


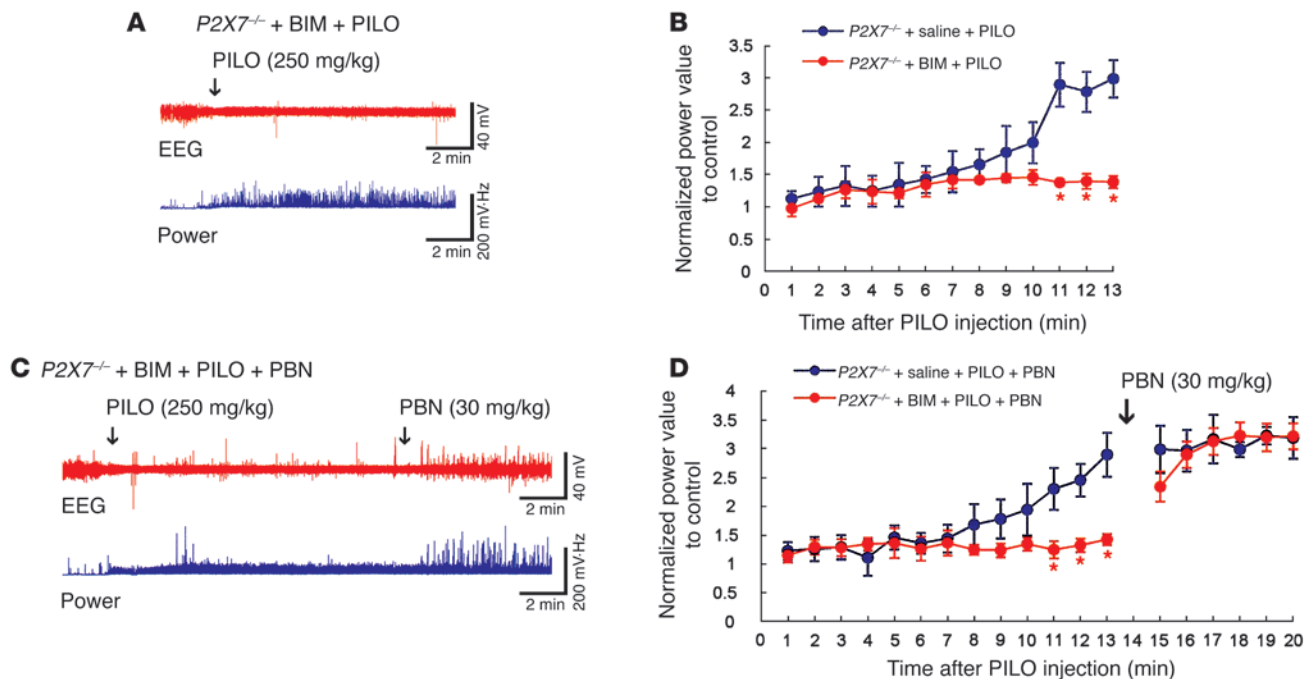
Figure 7

ICR-related molecules in the hippocampi of WT and P2X7^{-/-} mice. (A) Protein expressions for the IP3 receptor, ryanodine receptor, and SERCA2 ATPase. (B–D) Optical density of (B) the IP3 receptor, (C) the ryanodine receptor, and (D) SERCA2 ATPase, based on Western blotting (n = 5). (E–J) Immunoreactivity of (E) the IP3 receptor, (G) the ryanodine receptor, and (I) SERCA2 ATPase. Scale bar: 400 μm. Optical density of (F) the IP3 receptor, (H) the ryanodine receptor, and (J) SERCA2 ATPase, based on immunohistochemistry (n = 5). (K) Effect of 2-APB pretreatment on EEGs and power values in P2X7^{-/-} mice after PILO injection. (L) Power values after PILO injection, normalized to control (n = 5). *P < 0.05 vs. saline. Data are mean ± SEM.

sense, 5'-UUUUAUGUUCUCCAGCACCTT-3'; (c) sense, 5'-GCUCAAUUC-GUACAAGUGUTT-3'; antisense, 5'-ACACUUGUACGAUUUGAGCTC-3'. A nonsilencing RNA, as indicated by Ambion Inc., was used as the control siRNA. The doses of drugs and siRNA were chosen based on preliminary studies indicating that administration of up to the chosen dose was well tolerated, and no signs of neurotoxicity (hind-limb paralysis, vocalization, food intake, or neuroanatomical damage) were observed.

Behavioral seizure activity. Mice were treated with KA (25 mg/kg i.p.), picrotoxin (5 mg/kg i.p.), or PILO (150, 175, 200, 225, or 250 mg/kg i.p.)

20 minutes after administration of scopolamine methylbromide (2 mg/kg i.p.) to reduce peripheral cholinergic effects. Mice matched for sex, age, and body weight received the same amount of saline as controls. In some animals, CBX (30 mg/kg i.p.), PBN (30 mg/kg i.p.), or saline (i.p.) was administered 30 minutes before PILO injection (250 mg/kg i.p.). Drug doses were chosen based on preliminary studies. Mice were monitored continuously for 5 hours to register onset and extent of seizure activity. Seizures were scored as follows: 0, normal; 1, immobilization; 2, rearing and falling; 3, seizure for less than 1 hour; 4, seizure for 1–3 hours; 5, seizure for more than 3 hours; 6, death.

**Figure 8**

Effect of PKC inhibition on PILO-induced seizure susceptibility in $P2X7^{-/-}$ mice. (A) Effect of PKC inhibition on EEGs and power values in $P2X7^{-/-}$ mice after PILO injection. (B) Power values after PILO injection, normalized to control ($n = 5$). (C) Effect of PBN treatment on PKC inhibition-mediated reduction on EEGs and power values in $P2X7^{-/-}$ mice after PILO injection. (D) Power values after PILO injection, normalized to control ($n = 5$). Data are mean \pm SEM. * $P < 0.05$ vs. saline.

Electrophysiology. Mice were anesthetized (urethane, 1.5 g/kg i.p.) and placed in a stereotaxic frame. Holes were drilled through the skull to introduce electrodes. The coordinates for the recording electrode, relative to the dentate gyrus, were -2.0 mm anterior-posterior, 1.5 mm lateral to the bregma, and 2.0 mm deep, at a right angle to the skull surface. A stainless steel electrode (Plastics One Inc.) was used for recording. The reference electrode was placed in the posterior cranium over the cerebellum. Signals were recorded with a DAM 80 differential amplifier (0.1–3000 Hz band-pass; World Precision Instruments) and the data were digitized (400 Hz) and analyzed using MacChart 5 (AD Instruments). After establishing a stable baseline for at least 30 minutes, mice were injected with CBX (30 mg/kg i.p.), PBN (30 mg/kg i.p.), DAN (10 mg/kg i.p.), 2-APB (10 mg/kg i.p.), or saline (i.p.). 30 minutes after administration, PILO (250 mg/kg i.p.) was given. Drug doses were chosen based on preliminary studies.

Some of the animals were used for measurement of evoked responses in the dentate gyrus. The coordinates for the stimulating electrode, relative to the angular bundle, were -3.8 mm anterior-posterior, 2.0 mm lateral to the bregma, and 2.0 mm deep. Electrode depths were selected by optimizing the evoked response. Data were recorded with a DAM 80 differential amplifier, digitized (10 kHz), and analyzed using MacChart 5. Stimuli were applied as DC square pulses at 0.1 Hz with pairs of 100- μ s constant current stimuli at 20-, 30-, 70-, 150-, and 250-ms interstimulus intervals, depending on the threshold intensity evoking the population spike (~ 1 mV). After establishing a stable baseline for at least 30 minutes and a control IO curve, mice were injected i.p. with the drugs described above, and paired-pulse responses were measured.

Analysis. Time of seizure onset was defined as the time point showing paroxysmal depolarizing shift, defined as lasting more than 3 seconds and consisting of a rhythmic discharge of more than 2 Hz and usually between 4 and 10 Hz (42). The amplitude spectrum analysis power value (referred to

herein as the power value) was estimated by multiplying event amplitude (difference between the cyclic maximum and cyclic minimum value of an event, in mV) by event frequency (number of waveforms over detection threshold of an event [2 SD of cycles], in Hz), and the resulting power was expressed as mV \cdot Hz. To analyze changes in the power values, they were normalized to the average of the values obtained for WT animals (controls). The population spike amplitude was measured by projecting a line from the negative peak to a tangent line connecting the spike onset and offset, when 1.2 \times threshold stimulus intensity was applied. To analyze changes in the evoked responses, the average of the population spike amplitudes of the first response during the baseline measurement was used to normalize all population spike amplitude measurements during a recording session for an individual animal (43).

Anatomy. Control and test animals were perfused via the ascending aorta with 200 ml 4% paraformaldehyde in phosphate buffer (PB). The brains were removed, postfixed in the same fixative for 4 hours, and rinsed in PB containing 30% sucrose at 4 $^{\circ}$ C for 2 days. Thereafter, the tissues were frozen, 30- μ m-thick sections were obtained using a cryostat, and consecutive sections were collected in 6-well plates containing PBS. These free-floating sections were first incubated with 10% normal horse serum for 30 minutes at room temperature. They were then incubated with rabbit anti-M1 receptor IgG (M1 receptor, diluted 1:200; Millipore), ryanodine receptor IgG (diluted 1:1,000; Abcam), Panx1 IgG (diluted 1:500; Millipore), IP3 receptor IgG (diluted 1:1,000; Abcam), SERCA2 ATPase IgG (diluted 1:500; Abcam), VGAT IgG (diluted 1:500; Millipore), or guinea pig anti-VGLUT IgG (diluted 1:1,000; Millipore) in PBS containing 0.3% triton X-100 and 2% normal chicken serum overnight at room temperature. After washing 3 times for 10 minutes with PBS, sections were incubated sequentially with the secondary antibody and ABC complex (Vector Laboratories Inc.), diluted 1:200 in the same solution as the primary antiserum. Between incubations, tissues were washed with PBS 3 times for 10 minutes each. The

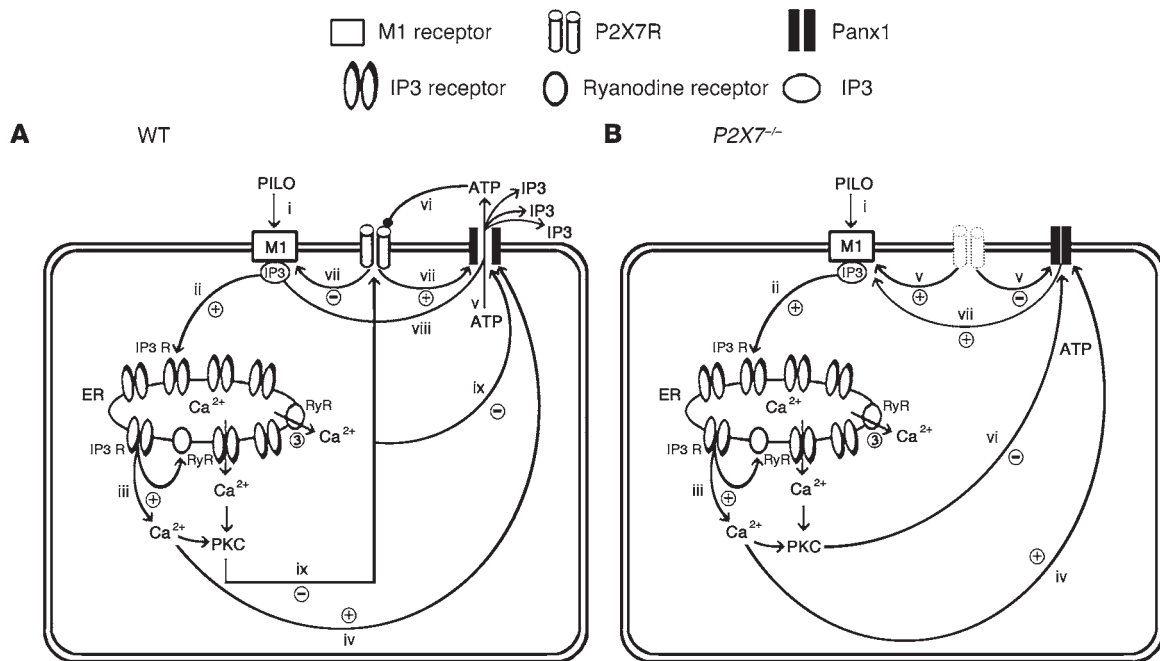


Figure 9

Hypothesized role of the P2X7R-Panx1 complex in regulating M1 receptor activity. **(A)** In WT mice, M1 receptor activation triggers IP3 production and increases ICR (i–iii). Elevated intracellular Ca²⁺ contributes to opening Panx1 (iv), which allows IP3 clearance, Ca²⁺ wave propagation, and ATP release (v). Releasing ATP through Panx1 activates P2X7R (vi), which desensitizes the M1 receptor and sustains Panx1 opening for clearance of IP3 (vii and viii). In turn, PKC activation leads to closure of P2X7R and Panx1 (ix). **(B)** In P2X7^{-/-} mice, M1 receptor activation triggers ICR via IP3 production (i–iii). Elevated intracellular Ca²⁺ contributes to opening Panx1 (iv). In the absence of P2X7R, Panx1 opening and M1 receptor desensitization cannot be sustained (v). Simultaneously, PKC activation rapidly closes the Panx1 channel (vi), which induces accumulation of intracellular IP3 caused by failure of IP3 clearance and prolonged M1 receptor activation (vii). See Discussion for details.

sections were visualized using 3,3'-diaminobenzidine in 0.1 M Tris buffer and mounted on gelatin-coated slides. Double immunofluorescence for rabbit anti-Panx1 IgG (diluted 1:200; Millipore) and mouse anti-Panx1 IgG (diluted 1:200; Millipore) was also performed using the M.O.M. kit (Vector Laboratories) according to the manufacturer's protocol. Immunoreactions were observed using an Axio Scope microscope (Carl Zeiss). To establish the specificity of the immunostaining, a negative control test was carried out with preimmune serum instead of the primary antibody. No immunoreactivity was observed for the negative control in any structures. All experimental procedures in this study were performed under the same conditions and in parallel.

Western blot. After sacrifice, the hippocampus was obtained. Tissues were homogenized in 50 mM Tris containing 50 mM HEPES (pH 7.4), ethylene glycol tetraacetic acid (pH 8.0), 0.2% Tergitol type NP-40, 10 mM ethylenediaminetetraacetic acid (pH 8.0), 15 mM sodium pyrophosphate, 100 mM β-glycerophosphate, 50 mM NaF, 150 mM NaCl, 2 mM sodium orthovanadate, 1 mM phenylmethylsulfonyl fluoride, and 1 mM dithiothreitol. After centrifugation, the protein concentration in the supernatant was determined using a Micro BCA Protein Assay Kit with bovine serum albumin as the standard (Pierce Chemical). Aliquots containing 20 μg total protein were boiled in a loading buffer containing 150 mM Tris (pH 6.8), 300 mM dithiothreitol, 6% sodium dodecyl sulfate, 0.3% bromophenol blue, and 30% glycerol. Each aliquot was then loaded onto a 10% polyacrylamide gel. After electrophoresis, gels were transferred to nitrocellulose transfer membranes (Schleicher and Schuell BioScience Inc.). To reduced background staining, the filters were incubated with 5% nonfat dry milk in PBS con-

taining 0.1% Tween 20 for 45 minutes, followed by incubation with rabbit anti-Panx1 (1:3,000), M1 receptor (1:200), ryanodine receptor (1:1,000), IP3 receptor (1:1,000), or SERCA2 ATPase (1:1,000) with peroxidase-conjugated goat anti-rabbit IgG. Western blotting was conducted with an ECL Western Blotting Detection Kit (Amersham) (44).

Quantification of immunohistochemistry and Western blotting. For quantification of immunohistochemical data, images of each section (including the molecular layer and the granule cell layer of the dentate gyrus; 5 sections per animal) were captured. Each image was normalized by adjusting the black and white range using Photoshop (version 8.0; Adobe). Intensity measurements were represented as the mean grayscale value on a 256 gray-level scale (using NIH Image 1.59 software). Values for background staining were obtained from the corpus callosum. Optical density values obtained from immunohistochemistry and Western blotting images were corrected by subtracting the average value for background noise from 5 image inputs. The optical density was then standardized by setting the threshold levels.

Statistics. All data were analyzed using 2-tailed Student's *t* test or 1-way ANOVA to determine statistical significance. Bonferroni's test was used for post-hoc comparisons. The incidence of seizure was analyzed using Fisher's exact test. A *P* value less than 0.05 was considered statistically significant.

Acknowledgments

This work was supported by grant A080007 from the Korea Healthcare Technology Research and Development Project of the Ministry for Health, Welfare, and Family Affairs of South



Korea and by grants R01-2008-000-20128-0, 2009-0093812, and 2010K000808 from the National Research Foundation of Korea.

Received for publication August 19, 2010, and accepted in revised form March 2, 2011.

Address correspondence to: Tae-Cheon Kang, Department of Anatomy and Neurobiology, College of Medicine, Hallym University, Chunchon, Kangwon-Do 200-702, South Korea. Phone: 82.33.248.2524; Fax: 82.33.248.2525; E-mail: tckang@hallym.ac.kr.

1. North RA. Molecular physiology of P2X receptors. *Physiol Rev.* 2002;82(4):1013–1067.
2. Ferrari D, et al. The P2X7 receptor: a key player in IL-1 processing and release. *J Immunol.* 2006;176(7):3877–3883.
3. Locovei S, Scemes E, Qiu F, Spray DC, Dahl G. Pannexin1 is part of the pore forming unit of the P2X7R death complex. *FEBS Lett.* 2007;581(3):483–488.
4. Pelegrin P, Surprenant A. Pannexin-1 mediates large pore formation and interleukin-1 β release by the ATP-gated P2X7 receptor. *EMBO J.* 2006;25(21):5071–5082.
5. Panchin Y, Kelmanson I, Matz M, Lukyanov K, Usman N, Lukyanov S. A ubiquitous family of putative gap junction molecules. *Curr Biol.* 2000;10(13):R473–R474.
6. Dahl G, Locovei S. Pannexin: to gap or not to gap, is that a question? *IUBMB Life.* 2006;58(7):409–419.
7. Huang Y, Grinspan JB, Abrams CK, Scherer SS. Pannexin1 is expressed by neurons and glia but does not form functional gap junctions. *Glia.* 2007;55(1):46–56.
8. Thompson RJ, Zhou N, MacVicar BA. Ischemia opens neuronal gap junction hemichannels. *Science.* 2006;312(5775):924–927.
9. Thompson RJ, et al. Activation of pannexin-1 hemichannels augments aberrant bursting in the hippocampus. *Science.* 2008;322(5907):1555–1559.
10. Qiu F, Dahl G. A permeant regulating its permeation pore: inhibition of pannexin1 channels by ATP. *Am J Physiol Cell Physiol.* 2009;296(2):C250–C255.
11. Vreugdenhil M, Toescu EC. Age-dependent reduction of gamma oscillations in the mouse hippocampus in vitro. *Neuroscience.* 2005;132(4):1151–1157.
12. Hamilton SE, et al. Disruption of the m1 receptor gene ablates muscarinic receptor-dependent M current regulation and seizure activity in mice. *Proc Natl Acad Sci U S A.* 1997;94(24):13311–13316.
13. Gigout S, Louvel J, Pumain R. Effects in vitro and in vivo of a gap junction blocker on epileptiform activities in a genetic model of absence epilepsy. *Epilepsy Res.* 2006;69(1):15–29.
14. Taylor CP, Vartanian MG. Probenecid pretreatment enhances anticonvulsant action of NBQX in mice. *Eur J Pharmacol.* 1992;213(1):151–153.
15. Iglesias R, et al. P2X7 receptor-Pannexin1 complex: pharmacology and signaling. *Am J Physiol Cell Physiol.* 2008;295(3):C752–C760.
16. Tang FR, Lee WL, Gao H, Chen Y, Loh YT, Chia SC. Expression of different isoforms of protein kinase C in the rat hippocampus after pilocarpine-induced status epilepticus with special reference to CA1 area and the dentate gyrus. *Hippocampus.* 2004;14(1):87–98.
17. Liu JX, Tang YC, Liu Y, Tang FR. mGluR5-PLCbeta4-PKCbeta2/PKCgamma pathways in hippocampal CA1 pyramidal neurons in pilocarpine model of status epilepticus in mGluR5+/+ mice. *Epilepsy Res.* 2008;82(2–3):111–123.
18. Pelegrin P, Surprenant A. Pannexin-1 couples to maitotoxin- and nigericin-induced interleukin-1 β release through a dye uptake independent pathway. *J Biol Chem.* 2007;282(4):2386–2394.
19. Scemes E, Suadicani SO, Dahl G, Spray DC. Connexin and pannexin mediated cell-cell communication. *Neuron Glia Biol.* 2007;3(3):199–208.
20. Suadicani SO, Brosnan CF, Scemes E. P2X7 receptors mediate ATP release and amplification of astrocytic intercellular Ca²⁺ signaling. *J Neurosci.* 2006;26(5):1378–1385.
21. Locovei S, Bao L, Dahl G. Pannexin1 in erythrocytes: function without a gap. *Proc Natl Acad Sci U S A.* 2006;103(20):7655–7659.
22. Huang YJ, Maruyama Y, Dvoryanchikov G, Pereira E, Chaudhari N, Roper SD. The role of pannexin1 hemichannels in ATP release and cell-cell communication in mouse taste buds. *Proc Natl Acad Sci U S A.* 2007;104(15):6436–6441.
23. Locovei S, Wang J, Dahl G. Activation of pannexin1 channels by ATP through P2Y receptors and by cytoplasmic calcium. *FEBS Lett.* 2006;580(1):239–244.
24. Parpura V, Scemes E, Spray DC. Mechanisms of glutamate release from astrocytes: gap junction “hemichannels”, purinergic receptors and exocytotic release. *Neurochem Int.* 2004;45(2–3):259–264.
25. Di Iorio P, Ballerini P, Caciagli F, Ciccarelli R. Purinoceptor-mediated modulation of purine and neurotransmitter release from nervous tissue. *Pharmacol Res.* 1998;37(3):169–178.
26. Cotrina ML, Lin JH, Lopez-Garcia JC, Naus CC, Nedergaard M. ATP-mediated glia signaling. *J Neurosci.* 2000;20(8):2835–2844.
27. Sanderson MJ, Charles AC, Boitano S, Dirksen ER. Mechanisms and function of intercellular calcium signaling. *Mol Cell Endocrinol.* 1994;98(2):173–187.
28. Boitano S, Dirksen ER, Sanderson MJ. Intercellular propagation of calcium waves mediated by inositol trisphosphate. *Science.* 1992;258(5080):292–295.
29. Saez JC, Connor JA, Spray DC, Bennett MV. Hepatocyte gap junctions are permeable to the second messenger, inositol 1,4,5-trisphosphate, and to calcium ions. *Proc Natl Acad Sci U S A.* 1989;86(8):2708–2712.
30. Bruzzone R, Barbe MT, Jakob NJ, Monyer H. Pharmacological properties of homomeric and heteromeric pannexin hemichannels expressed in *Xenopus* oocytes. *J Neurochem.* 2005;92(5):1033–1043.
31. Vanden Abeele F, et al. Functional implications of calcium permeability of the channel formed by pannexin1. *J Cell Biol.* 2006;174(4):535–546.
32. Fukushi Y. Heterologous desensitization of muscarinic receptors by P2Z purinoceptors in rat parotid acinar cells. *Eur J Pharmacol.* 1999;364(1):55–64.
33. Nakamoto T, Brown DA, Catalán MA, Gonzalez-Begne M, Romanenko VG, Melvin JE. Purinergic P2X7 receptors mediate ATP-induced saliva secretion by the mouse submandibular gland. *J Biol Chem.* 2009;284(8):4815–4822.
34. Zündorf G, Kahler S, Reiser G. Gap-junction blocker carbenoxolone differentially enhances NMDA-induced cell death in hippocampal neurons and astrocytes in co-culture. *J Neurochem.* 2007;102(2):508–521.
35. Jellinck PH, Monder C, McEwen BS, Sakai RR. Differential inhibition of 11 beta-hydroxysteroid dehydrogenase by carbenoxolone in rat brain regions and peripheral tissues. *J Steroid Biochem Mol Biol.* 1993;46(2):209–213.
36. van Haarst AD, Welberg LA, Sutanto W, Oitzl MS, de Kloet ER. 11 beta-Hydroxysteroid dehydrogenase activity in the hippocampus: implications for in vivo corticosterone receptor binding and cell nuclear retention. *J Neuroendocrinol.* 1996;8(8):595–600.
37. Contreras JE, et al. Metabolic inhibition induces opening of unopposed connexin 43 gap junction hemichannels and reduces gap junctional communication in cortical astrocytes in culture. *Proc Natl Acad Sci U S A.* 2002;99(1):495–500.
38. Kim DY, Kam Y, Koo SK, Joe CO. Gating connexin 43 channels reconstituted in lipid vesicles by mitogen-activated protein kinase phosphorylation. *J Biol Chem.* 1999;274(9):5581–5587.
39. Moreno AP. Connexin phosphorylation as a regulatory event linked to channel gating. *Biochim Biophys Acta.* 2005;1711(2):164–171.
40. Bradford MD, Soltoff SP. P2X7 receptors activate protein kinase D and p42/p44 mitogen-activated protein kinase (MAPK) downstream of protein kinase C. *Biochem J.* 2002;366(pt 3):745–755.
41. Hung AC, et al. Roles of protein kinase C in regulation of P2X7 receptor-mediated calcium signalling of cultured type-2 astrocyte cell line, RBA-2. *Cell Signal.* 2005;17(11):1384–1396.
42. Rutecki PA, Yang Y. Ictal epileptiform activity in the CA3 region of hippocampal slices produced by pilocarpine. *J Neurophysiol.* 1998;79(6):3019–3029.
43. Kim JE, et al. Anti-glutamatergic effect of riluzole: comparison with valproic acid. *Neuroscience.* 2007;147(1):136–145.
44. Kim JE, Kim DW, Kwak SE, Kwon OS, Choi SY, Kang TC. Potential role of pyridoxal-5'-phosphate phosphatase/chronopin in epilepsy. *Exp Neurol.* 2008;211(1):128–140.